Sonosensitizers with Various Imaging Functions

Subjects: Medicine, General & Internal

Contributor: Mingxin Zhang , Yunlong Liang , Mingzhen Zhang , Yujie Zhang

With the rapid development of sonodynamic therapy (SDT), sonosensitizers have evolved from traditional treatments to comprehensive diagnostics and therapies. Sonosensitizers play a crucial role in the integration of ultrasound imaging (USI), X-ray computed tomography (CT), and magnetic resonance imaging (MRI) diagnostics while also playing a therapeutic role.

sonodynamic therapy sonosensitizers clinical

1. Contrast-Enhanced Ultrasound (CEUS)

Ultrasound (US) is a sound wave with a frequency of more than 20,000 Hz that is inaudible to the human ear. Ultrasound has the advantages of low-cost, simple, rapid, non-invasive, non-radioactive, accurate, continuous, dynamic, and repeatable scans [1][2][3]. Using the physical properties of ultrasound, various cross-sectional images of organs and surrounding organs can be displayed, which is close to the anatomical real structure. Therefore, ultrasound is often used as the first choice for the examination of solid organs and fluid-containing organs. In particular, ultrasound elastography and contrast-enhanced ultrasound (CEUS) are well established as being used for diagnosis. In CEUS, intravenously injected microbubbles are excited by longitudinal ultrasound in the examined area, producing nonlinear oscillations. The corresponding contrast agent software can distinguish the diseased tissues from the received contrast agent signals [4]. However, currently, 78.5% of radiology departments use diagnostic ultrasound imaging as a routine diagnostic imaging method, while only 26% of them use contrast-enhanced ultrasound [4]. The excessively expensive price of ultrasound contrast agents and their lower selectivity limited the clinical application of CEUS. It was found that some sonosensitizers used for SDT treatment also showed promising results in CEUS. **Table 1** lists the sonosensitizers and imaging capabilities used for CEUS imaging. Sonosensitizers produce stable microbubbles (MBs) or nanobubbles (NBs) under CEUS cavitation to achieve enhanced imaging [5][6][7]. Sonosensitizers achieve synergistic drug delivery and tumor therapy by affecting the lesion's tissue structure. Therefore, with the development of sonosensitizers, the clinical application of contrast-enhanced ultrasound is becoming more and more broad.

Table 1. US Imaging Characteristics of the Multifunctional Sonosensitizers.

Sonosensitizers	Probes	Biological Model	SDT Result	Imaging Effect	Ref.
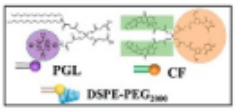 PCF-MBs	PCF	HT-29 cancer-bearing Balb/c nude mice	tumor inhibition rate of more than 50%	20 s post-injection, the US imaging signal reached the maximum; and the contrast enhancement could last for more than 3 min	[8]
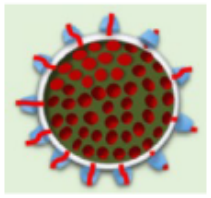 FMSN-DOX	FMSNs	TRAMP tumor-bearing nude mice	The gradual reduction in tumor growth	from day 1 to day 9 with significant contrast enhancement within the tumor.	[9]
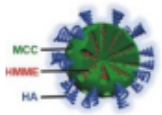 HMME/MCC-HA	MCC NPs	MCF-7 tumor-bearing nude mice	successfully suppressed the tumor volume with the V/V0 of 0.87 ± 0.13	strong US signals in tumor site at 3 h post-injection, and particularly after exposure to US stimulus	[10]
 Lip-AIPH	AIPH	MCF-7 tumor-bearing mice	a highly significant antitumor effect was achieved in mice in the group of Lip-AIPH with US irradiation	a highly significant antitumor effect was achieved in mice in the group of Lip-AIPH with US irradiation	[11]
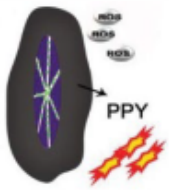 $mTiO_2$@PPY-HNK	$mTiO_2$	4T1 tumor model	significantly inhibit the tumor growth	as the concentration increases, the ultrasound signal is more intense and the image is clearer	[12]
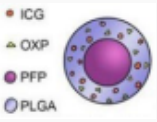 OIX_NPs	PFP	ID8 cells into the left shoulder (the primary tumor)	significant inhibition of tumor volume	peaking at 4 h post-injection.	[13]
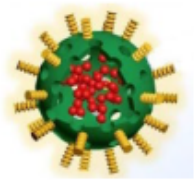 TPZ/HMTNPs-SNO	HMTNPs-SNO	MCF-7 tumor-bearing nude mice	exhibited an effective therapeutic effect	compared with the saline group, showed local enhancement at the tumor site.	[14]

Sonosensitizers	Probes	Biological Model	SDT Result	Imaging Effect	Ref.
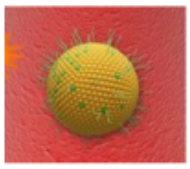 IR780-NDs	PFP	breast cancer 4T1 nude mice	Tumor weight drop	24 h after the injection of IR780-NDs a bright US signal occurred at the tumor site.	[15]
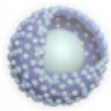 SMISO NPs	SMISO	4T1 tumor-bearing nude mice	the inhibition rate of tumor growth in the SMISO + US group reached 88.2%	the grayscale values of US images increase with them. concentration increases	[16]
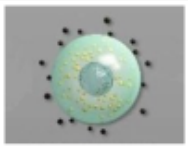 RPPs&SPIOs [8]	RPPs	4T1 tumors	a 100% survival rate of mice at 90 days	Shift in RPPs after thermal stimulation results in significant contrast enhancement	[17]
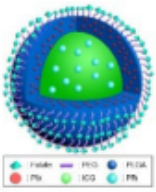 FA-PEG-PLGA-Ptx@ICG-Pfh NPs	Pfh	MDA-MB231 tumor-bearing mice	tumor growth was significantly inhibited	images were greatly improved	[18]
 [16] RBC-HPBs/HMME/PFH	PFH	4T1 tumor-bearing female mice	enhancing tumor treatment effects of HMME	2 3A clear US signal was observed at 4 h after injection, and the strongest signal appeared at 8 h.	[19]
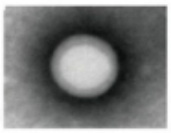 Ce6-PFP-DTX/PLGA	PFP	breast cancer 4T1 nude mice	much higher inhibition rate of the CPDP NPs + LIFU group	after LIFU irradiation, the corresponding intensity of CPDP NPs was elevated compared with the pre-irradiation group	[20]
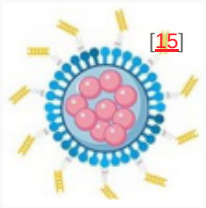 [15] AS1411-DOX-PFH-	PFH	breast cancer 4T1 nude mice	the tumor volumes significantly decreased	Increased imaging ability of ADPPs in vivo within 24 h after intravenous injection	[21]

robubbles odynamic -29 colon ltrasound umor. The

spinodal . The live r SMISO e control he signal ltrasound appeared, inhibited ty.

ing IR780 780-NDs, cer. At 24 lition, the n the pre-injection group.

Sonosensitizers	Probes	Biological Model	SDT Result	Imaging Effect	Ref.
PEG@PLGA					
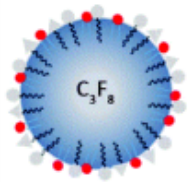 RB-MBs	MBs	HT-29 tumor mouse model	-	a contrast-enhanced ultrasound imaging mode at a frequency of 5 MHz	[22]

[23]

[24]

different

ninvasive

vided into

T cannot

xogenous

es. Iodine

contrast is commonly used in clinical practice but has the following limitations: (1) susceptibility to allergic reactions and nephrotoxicity; (2) low dose-efficiency ratio; and (3) lack of targeting. Studies have investigated the utilization of sonosensitizers as CT imaging agents to overcome the shortcomings of commonly used clinical contrast agents. **Table 2** lists the sonosensitizers and imaging capabilities used for CT imaging.

Table 2. CT Imaging Characteristics of the Multifunctional Sonosensitizers.

Sonosensitizers	Probes	Biological Model	Treatment Result	Imaging Effect	Ref.
 $MnWO_X$-PEG	$W(CO)_6$	4T1 tumor-bearing mice	Tumor weight drop	CT imaging signal intensity was almost 2.4 times higher than that of the control group	[25]
 $AgBiS_2$@DSPE-PEG_{2000}-FA	$AgBiS_2$	HeLa tumor-bearing mice	Tumor size drop	The CT signal intensity at the tumor site gradually increased and peaked at 6h after the injection	[26]
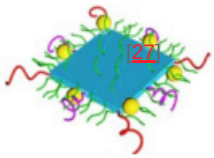 Au-TiO_2-A-TPP	Au-TiO_2	MCF-7 tumor-bearing mice	Tumor weight drop	The CT signal in the tumor area reached its maximum at 24 h	[27]

TPP) and

erapy for

als at the

tumor sites, which validated the capability of Au-TiO_2-A-TPP to diagnose tumors by CT imaging in vivo. As the concentration of Au-TiO_2-A-TPP increased, the brightness and CT values of CT images increased, suggesting a linear relationship between CT grayscale values and concentration. As mentioned previously, contrast agents commonly used in clinical practice may not be appropriate for patients with renal insufficiency, who may be better suited for contrast agents with a short half-life in vivo and low nephrotoxicity. Surprisingly, the half-life of Au-TiO_2-A-TPP in the blood circulation of mice was only 4.71 h, indicating Au-TiO_2-A-TPP was very promising for patients with renal insufficiency.

Sonosensitizers	Probes	Biological Model	Treatment Result	Imaging Effect	Ref.
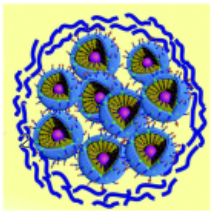 GMCDS-FA@CMC	$Au@mSiO_2$	orthotopic colorectal tumor	Decreased number and smaller diameter of colorectal tumors	The nanoprobe remained in the colorectal region	[28]

[26] targeted ound that e steadily eted ABS- ^{2}) infrared after drug

Zhang et al. [28] constructed a novel oral nanoparticle, $Au@mSiO_2$/Ce6/DOX/SLB-FA@CMC (GMCDS-FA@CMC), that endowed the pH/ultrasonic dual-response to realize the combination of SDT with chemotherapy for colorectal cancer treatment. After oral delivery of GMCDS-FA@CMC, a well-defined tumor CT signal was observed in situ in colorectal cancer model mice and persisted for 7–9 h. It was found that the enteric-coated particles possessed good CT imaging effects in vivo by oral delivery and could be used to direct SDT-chemotherapy for colorectal cancer treatment.

3. Magnetic Resonance Imaging (MRI)

Since the first implementation of MRI in 1973 as a non-invasive and multi-contrast detection method, MR imaging has been widely used in various biomedical fields [29]. MRI can reflect tissue lesions by combining parameters such as flow effects and electromagnetic wave-related proton density after the excitation of strong magnetic field pulses and the formation of magnetic resonance phenomena through hydrogen atoms in human water molecules [30]. The images are also processed with the aid of computer technology to obtain an excellent diagnosis of the pathology, which has high spatial and tissue resolution [31][32][33]. Therefore, it is extensively utilized clinically in the diagnosis and prognostic status of various diseases. Magnetic resonance imaging is not sensitive, but this obstacle can be overcome by exogenous contrast agents by decreasing the relaxation time of bulk water [33][34]. It was found that appropriate contrast agents are important for enhancing the susceptibility and specificity of diagnosis, enhancing the degree of signal contrast, and improving the resolution of soft tissue images for clinical application [29]. For example, with the help of gadolinium (Gd)-based T_1 agents, information about the boundaries of brain tumors can be observed more clearly [35]. In recent years, some new nuclear magnetic sensitizers containing Mn and Fe have been applied to MRI tumor imaging [36][37]. **Table 3** lists the sonosensitizers and imaging capabilities used for MRI imaging.

Table 3. MR Imaging Characteristics of the Multifunctional Sonosensitizers.

Sonosensitizers	Probes	Biological Model	SDT Result	Imaging Effect	Ref.
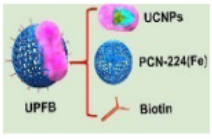 UPFB	MOFs (Fe^{3+})	U14 tumor-bearing Kunming mice	increased inhibition of tumor growth	enhanced T_2 contrast signal	[37]

Sonosensitizers	Probes	Biological Model	SDT Result	Imaging Effect	Ref.
 Fe-TiO_2 NDs	Fe^{3+}	4T1 tumor-bearing mice	better tumor inhibition	The brightening effect through the T_1-weighted MR images	[38]
 Fe-VS_2-PEG	Fe^{3+}	4T1 cells subcutaneously in BALB/c mice	better treatment effect and a longer survival period	the tumor had an obvious brightening effect 24 h after i.v. injection (T_1)	[36]
 OCN-PEG-(Ce6-Gd^{3+})/BNN6	Ga^{3+}	4T1 tumor-bearing mice	the tumor suppression rate reached 63.2%	The T_1-weighted contrast effect was significantly enhanced	[39]
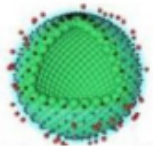 $MnSiO_3$-Pt@BSA-Ce6(MPBC)	Mn^{2+}	U14 tumor-bearing Balb/c mice	tumor growth inhibition	the T1−MR signal of the tumor enhanced	[40]
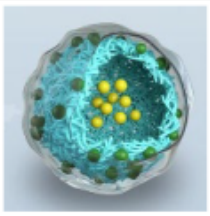 MG@P NPs	PMnC (Mn)	4T1 tumor-bearing mice	the tumor growth of Mice remarkably suppressed	T_1 signal of the tumor region showed an increasing trend within 24 h and then decreased	[41]
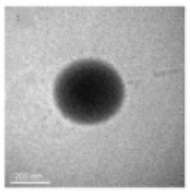 F3-PLGA@MB/Gd NPs	Gd-DTPA-BMA	the nude mice bearing MDA-MB-231 tumors	induce tumor cell apoptosis	Linear signal dependence of T_1 intensity values	[42]
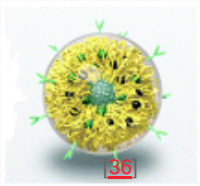 [35] Ang-IR780-MnO_2-PLGA (AIMP)	MnO_2	U87MG tumor-bearing mice	enhanced SDT effect	A linear relationship was shown between the $1/T_1$ values and Mn concentration	[43]

ensitizers (CDT) for cancer therapy. Fe-VS_2-PEG NSs have magnetic resonance imaging capability and strong tumor inhibitity in vivo. At 24 h after intravenous administration of Fe-VS_2-PEG, MR imaging of the tumor demonstrated significant enhancement, and the quantitative analysis showed that signal strength was 2.04 times stronger than that before

Sonosensitizers	Probes	Biological Model	SDT Result	Imaging Effect	Ref.
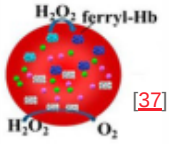 DOX/Mn-TPPS@RBCS	Mn-TPPS	MCF-7 tumor-bearing nude mice	Inhibit tumor growth	T_1-weighted MR imaging results in enhancement	[44]
 MnTTP-HSA	MnTTP (Mn)	MCF-7 tumor-bearing nude mice	the best in completely inhibiting tumor	a T_1 the positive signal at the tumor showed an increasing trend within 3 h and then gradually decreased	[45]
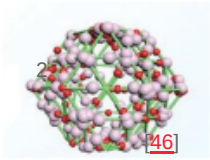 mZMD	MnO_2	HeLa tumor xenograft-bearing nude mice	significant suppression effects	the concentration of the NCs increased, the T_1 MR images became brighter and brighter	[46]
 GdHF-NDs	Ga^{3+}	CT26 tumor-bearing mice	GdHF-NDs/PEG + US shows the most potent efficiency in tumor suppression (73.7%)	T_1 signal strength increased	[31]

4. Multi-Modal Imaging

All imaging methods have their disadvantages: MRI has the characteristics of long acquisition time and low space coverage; CT has the risk of ionizing radiation; and the US has limited penetration ability [47][48][49][50]. Single-modality imaging cannot meet the growing demand for accuracy and reliability in clinical diagnostics or clinical research [51]. The combined application of multiple testing techniques has become a hot research topic, complementing each other's advantages and realizing more precise diseases [52]. Compared with single-mode imaging, multimode imaging achieves multiple imaging functions through a single nanomaterial, providing a basis for accurate cancer diagnosis [53]. To date, several nanoparticle-based bimodal co-imaging materials have been reported to achieve better imaging and treatment.

Wang et al. [54] prepared hollow CoP@N-carbon@PEG (CPCs@PEG) nanospheres (~60 nm) as sonosensitizers to inhibit tumor growth by promoting ROS production under US irradiation. With the incorporation of cobalt ions, which had magnetic properties and X-ray attenuation coefficients, CPCs@PEG were capable of both CT and MRI. Further, the authors also performed MRI imaging studies in vivo using 4T1 tumor-bearing mice as a model. After the injection of CPC10@PEG, the contrast of the cancer site became darker. In addition, the researchers conducted a CT imaging capability study. With the increase in CPC10@PEG concentration, the CT signal was gradually enhanced. The researchers also investigated the in vivo CT imaging capabilities of CPC10@PEG, which

showed a significant increase in the brightness of the cancer site after intravenous injection compared with pre-injection.

Gong et al. [25] designed and prepared a novel high-performance multifunctional sonosensitizer built on ultramicroscopic oxygen-deficient bimetallic oxide $MnWO_X$ nanoparticles for multimodal imaging-guided SDT for cancer therapy. The $MnWO_X$-PEG nanoparticles exhibited effective SDT effects by producing $^1O_2$ and ·OH and possessed the glutathione depletion capability to enhance the SDT efficacy. $MnWO_X$-PEG exhibited good biosafety and excellent tumor growth suppression in mice under ultrasound irradiation. Due to the high attenuation of X-rays by the W element, $MnWO_X$-PEG can also be applied in CT imaging and as a reduction agent for T_1 in magnetic resonance imaging. The findings indicated that after 24 h of intravenous injection of $MnWO_X$-PEG 4T1, the tumor-bearing mice showed significant CT (2.4 times) and MRI (1.8 times) signals in the tumor site. These multimodal imaging results demonstrated that $MnWO_X$-PEG can efficiently accumulate in tumors, and sonosensitizers had diagnostic imaging capabilities and assisted in the precise treatment of tumors with SDT.

References

1. Ke, H.; Wang, J.; Dai, Z.; Jin, Y.; Qu, E.; Xing, Z.; Guo, C.; Yue, X.; Liu, J. Gold-nanoshelled microcapsules: A theranostic agent for ultrasound contrast imaging and photothermal therapy. Angew. Chem. 2011, 50, 3017–3021.
2. Slagle, C.J.; Thamm, D.H.; Randall, E.K.; Borden, M.A. Click Conjugation of Cloaked Peptide Ligands to Microbubbles. Bioconjugate Chem. 2018, 29, 1534–1543.
3. Wang, Y.; Cong, H.; Wang, S.; Yu, B.; Shen, Y. Development and application of ultrasound contrast agents in biomedicine. J. Mater. Chem. B 2021, 9, 7633–7661.
4. Kloth, C.; Kratzer, W.; Schmidberger, J.; Beer, M.; Clevert, D.A.; Graeter, T. Ultrasound 2020—Diagnostics & Therapy: On the Way to Multimodal Ultrasound: Contrast-Enhanced Ultrasound (CEUS), Microvascular Doppler Techniques, Fusion Imaging, Sonoelastography, Interventional Sonography. In RöFo-Fortschritte auf dem Gebiet der Röntgenstrahlen und der Bildgebenden Verfahren; Georg Thieme Verlag KG: Leipzig, Germany, 2021; Volume 193, pp. 23–32.
5. Claudon, M.; Dietrich, C.F.; Choi, B.I.; Cosgrove, D.O.; Kudo, M.; Nolsøe, C.P.; Piscaglia, F.; Wilson, S.R.; Barr, R.G.; Chammas, M.C.; et al. Guidelines and good clinical practice recommendations for Contrast Enhanced Ultrasound (CEUS) in the liver—Update 2012: A WFUMB-EFSUMB initiative in cooperation with representatives of AFSUMB, AIUM, ASUM, FLAUS and ICUS. Ultrasound Med. Biol. 2013, 39, 187–210.
6. Huynh, E.; Rajora, M.A.; Zheng, G. Multimodal micro, nano, and size conversion ultrasound agents for imaging and therapy. Wiley Interdiscip. Rev. Nanomed. Nanobiotechnol. 2016, 8, 796–813.

7. Sun, S.; Xu, Y.; Fu, P.; Chen, M.; Sun, S.; Zhao, R.; Wang, J.; Liang, X.; Wang, S. Ultrasound-targeted photodynamic and gene dual therapy for effectively inhibiting triple negative breast cancer by cationic porphyrin lipid microbubbles loaded with HIF1α-siRNA. Nanoscale 2018, 10, 19945–19956.
8. Chen, M.; Liang, X.; Gao, C.; Zhao, R.; Zhang, N.; Wang, S.; Chen, W.; Zhao, B.; Wang, J.; Dai, Z. Ultrasound Triggered Conversion of Porphyrin/Camptothecin-Fluoroxyuridine Triad Microbubbles into Nanoparticles Overcomes Multidrug Resistance in Colorectal Cancer. ACS Nano 2018, 12, 7312–7326.
9. Ho, Y.J.; Wu, C.H.; Jin, Q.F.; Lin, C.Y.; Chiang, P.H.; Wu, N.; Fan, C.H.; Yang, C.M.; Yeh, C.K. Superhydrophobic drug-loaded mesoporous silica nanoparticles capped with β-cyclodextrin for ultrasound image-guided combined antivascular and chemo-sonodynamic therapy. Biomaterials 2020, 232, 119723.
10. Feng, Q.; Zhang, W.; Yang, X.; Li, Y.; Hao, Y.; Zhang, H.; Hou, L.; Zhang, Z. pH/Ultrasound Dual-Responsive Gas Generator for Ultrasound Imaging-Guided Therapeutic Inertial Cavitation and Sonodynamic Therapy. Adv. Healthc. Mater. 2018, 7, 1700957.
11. Lin, X.; Qiu, Y.; Song, L.; Chen, S.; Chen, X.; Huang, G.; Song, J.; Chen, X.; Yang, H. Ultrasound activation of liposomes for enhanced ultrasound imaging and synergistic gas and sonodynamic cancer therapy. Nanoscale Horiz. 2019, 4, 747–756.
12. He, Y.; Wan, J.; Yang, Y.; Yuan, P.; Yang, C.; Wang, Z.; Zhang, L. Multifunctional Polypyrrole-Coated Mesoporous TiO2 Nanocomposites for Photothermal, Sonodynamic, and Chemotherapeutic Treatments and Dual-Modal Ultrasound/Photoacoustic Imaging of Tumors. Adv. Healthc. Mater. 2019, 8, e1801254.
13. Zheng, J.; Sun, J.; Chen, J.; Zhu, S.; Chen, S.; Liu, Y.; Hao, L.; Wang, Z.; Chang, S. Oxygen and oxaliplatin-loaded nanoparticles combined with photo-sonodynamic inducing enhanced immunogenic cell death in syngeneic mouse models of ovarian cancer. J. Control. Release 2021, 332, 448–459.
14. Feng, Q.; Li, Y.; Yang, X.; Zhang, W.; Hao, Y.; Zhang, H.; Hou, L.; Zhang, Z. Hypoxia-specific therapeutic agents delivery nanotheranostics: A sequential strategy for ultrasound mediated on-demand tritherapies and imaging of cancer. J. Control. Release 2018, 275, 192–200.
15. Zhang, L.; Yi, H.; Song, J.; Huang, J.; Yang, K.; Tan, B.; Wang, D.; Yang, N.; Wang, Z.; Li, X. Mitochondria-Targeted and Ultrasound-Activated Nanodroplets for Enhanced Deep-Penetration Sonodynamic Cancer Therapy. ACS Appl. Mater. Interfaces 2019, 11, 9355–9366.
16. Zhang, T.; Zheng, Q.; Xie, C.; Fan, G.; Wang, Y.; Wu, Y.; Fu, Y.; Huang, J.; Craig, D.Q.M.; Cai, X.; et al. Integration of Silica Nanorattles with Manganese-Doped In2S3/InOOH to Enable Ultrasound-Mediated Tumor Theranostics. ACS Appl. Mater. Interfaces 2023, 15, 4883–4894.

17. Qin, Q.; Zhou, Y.; Li, P.; Liu, Y.; Deng, R.; Tang, R.; Wu, N.; Wan, L.; Ye, M.; Zhou, H.; et al. Phase-transition nanodroplets with immunomodulatory capabilities for potentiating mild magnetic hyperthermia to inhibit tumour proliferation and metastasis. J. Nanobiotechnol. 2023, 21, 131.
18. Liu, F.; Chen, Y.; Li, Y.; Guo, Y.; Cao, Y.; Li, P.; Wang, Z.; Gong, Y.; Ran, H. Folate-receptor-targeted laser-activable poly(lactide-co-glycolic acid) nanoparticles loaded with paclitaxel/indocyanine green for photoacoustic/ultrasound imaging and chemo/photothermal therapy. Int. J. Nanomed. 2018, 13, 5139–5158.
19. Zhang, H.; Chen, J.; Zhu, X.; Ren, Y.; Cao, F.; Zhu, L.; Hou, L.; Zhang, H.; Zhang, Z. Ultrasound induced phase-transition and invisible nanobomb for imaging-guided tumor sonodynamic therapy. J. Mater. Chem. B 2018, 6, 6108–6121.
20. Zhang, Q.; Wang, W.; Shen, H.; Tao, H.; Wu, Y.; Ma, L.; Yang, G.; Chang, R.; Wang, J.; Zhang, H.; et al. Low-Intensity Focused Ultrasound-Augmented Multifunctional Nanoparticles for Integrating Ultrasound Imaging and Synergistic Therapy of Metastatic Breast Cancer. Nanoscale Res. Lett. 2021, 16, 73.
21. Kang, Z.; Yang, M.; Feng, X.; Liao, H.; Zhang, Z.; Du, Y. Multifunctional Theranostic Nanoparticles for Enhanced Tumor Targeted Imaging and Synergistic FUS/Chemotherapy on Murine 4T1 Breast Cancer Cell. Int. J. Nanomed. 2022, 17, 2165–2187.
22. Hou, R.; Liang, X.; Li, X.; Zhang, X.; Ma, X.; Wang, F. In situ conversion of rose bengal microbubbles into nanoparticles for ultrasound imaging guided sonodynamic therapy with enhanced antitumor efficacy. Biomater. Sci. 2020, 8, 2526–2536.
23. Jiang, Z.; Zhang, M.; Li, P.; Wang, Y.; Fu, Q. Nanomaterial-based CT contrast agents and their applications in image-guided therapy. Theranostics 2023, 13, 483–509.
24. Pan, X.; Siewerdsen, J.; La Riviere, P.J.; Kalender, W.A. Anniversary paper. Development of x-ray computed tomography: The role of medical physics and AAPM from the 1970s to present. Med. Phys. 2008, 35, 3728–3739.
25. Gong, F.; Cheng, L.; Yang, N.; Betzer, O.; Feng, L.; Zhou, Q.; Li, Y.; Chen, R.; Popovtzer, R.; Liu, Z. Ultrasmall Oxygen-Deficient Bimetallic Oxide MnWOX Nanoparticles for Depletion of Endogenous GSH and Enhanced Sonodynamic Cancer Therapy. Adv. Mater. 2019, 31, e1900730.
26. Cheng, K.; Zhang, R.Y.; Yang, X.Q.; Zhang, X.S.; Zhang, F.; An, J.; Wang, Z.Y.; Dong, Y.; Liu, B.; Zhao, Y.D.; et al. One-for-All Nanoplatform for Synergistic Mild Cascade-Potentiated Ultrasound Therapy Induced with Targeting Imaging-Guided Photothermal Therapy. ACS Appl. Mater. Interfaces 2020, 12, 40052–40066.
27. Cao, Y.; Wu, T.; Dai, W.; Dong, H.; Zhang, X. TiO2 Nanosheets with the Au Nanocrystal-Decorated Edge for Mitochondria-Targeting Enhanced Sonodynamic Therapy. Chem. Mater.

2019, 31, 9105–9114.

28. Zhang, R.Y.; Cheng, K.; Xuan, Y.; Yang, X.Q.; An, J.; Hu, Y.G.; Liu, B.; Zhao, Y.D. A pH/ultrasonic dual-response step-targeting enterosoluble granule for combined sonodynamic-chemotherapy guided via gastrointestinal tract imaging in orthotopic colorectal cancer. Nanoscale 2021, 13, 4278–4294.
29. Guo, L.; Xi, J.; Teng, J.; Wang, J.; Chen, Y. Magnetic Resonance Neuroimaging Contrast Agents of Nanomaterials. Biomed. Res. Int. 2022, 2022, 6790665.
30. Yuan, P.; Song, D. MRI tracing non-invasive TiO2-based nanoparticles activated by ultrasound for multi-mechanism therapy of prostatic cancer. Nanotechnology 2018, 29, 125101.
31. Geng, P.; Yu, N.; Liu, X.; Zhu, Q.; Wen, M.; Ren, Q.; Qiu, P.; Zhang, H.; Li, M.; Chen, Z. Sub 5 nm Gd3+-Hemoporfin Framework Nanodots for Augmented Sonodynamic Theranostics and Fast Renal Clearance. Adv. Healthc. Mater. 2021, 10, e2100703.
32. Geethanath, S.; Vaughan, J.T., Jr. Accessible magnetic resonance imaging: A review. J. Magn. Reson. Imaging 2019, 49, e65–e77.
33. Pellico, J.; Ellis, C.M.; Davis, J.J. Nanoparticle-Based Paramagnetic Contrast Agents for Magnetic Resonance Imaging. Contrast Media Mol. Imaging 2019, 2019, 1845637.
34. De León-Rodríguez, L.M.; Martins, A.F.; Pinho, M.C.; Rofsky, N.M.; Sherry, A.D. Basic MR relaxation mechanisms and contrast agent design. J. Magn. Reson. Imaging 2015, 42, 545–565.
35. Abd-Ellah, M.K.; Awad, A.I.; Khalaf, A.A.M.; Hamed, H.F.A. A review on brain tumor diagnosis from MRI images: Practical implications, key achievements, and lessons learned. Magn. Reson. Imaging 2019, 61, 300–318.
36. Lei, H.; Wang, X.; Bai, S.; Gong, F.; Yang, N.; Gong, Y.; Hou, L.; Cao, M.; Liu, Z.; Cheng, L. Biodegradable Fe-Doped Vanadium Disulfide Theranostic Nanosheets for Enhanced Sonodynamic/Chemodynamic Therapy. ACS Appl. Mater. Interfaces 2020, 12, 52370–52382.
37. Wang, Z.; Liu, B.; Sun, Q.; Feng, L.; He, F.; Yang, P.; Gai, S.; Quan, Z.; Lin, J. Upconverted Metal-Organic Framework Janus Architecture for Near-Infrared and Ultrasound Co-Enhanced High Performance Tumor Therapy. ACS Nano 2021, 15, 12342–12357.
38. Bai, S.; Yang, N.; Wang, X.; Gong, F.; Dong, Z.; Gong, Y.; Liu, Z.; Cheng, L. Ultrasmall Iron-Doped Titanium Oxide Nanodots for Enhanced Sonodynamic and Chemodynamic Cancer Therapy. ACS Nano 2020, 14, 15119–15130.
39. Zheng, Y.; Liu, Y.; Wei, F.; Xiao, H.; Mou, J.; Wu, H.; Yang, S. Functionalized g-C3N4 nanosheets for potential use in magnetic resonance imaging-guided sonodynamic and nitric oxide combination therapy. Acta Biomater. 2021, 121, 592–604.

40. Jiang, F.; Yang, C.; Ding, B.; Liang, S.; Zhao, Y.; Cheng, Z.; Liu, M.; Xing, B.; Ma, P.; Lin, J. Tumor microenvironment-responsive MnSiO3-Pt@BSA-Ce6 nanoplatform for synergistic catalysis-enhanced sonodynamic and chemodynamic cancer therapy. Chin. Chem. Lett. 2022, 33, 2959–2964.
41. Wang, J.; Huang, J.; Zhou, W.; Zhao, J.; Peng, Q.; Zhang, L.; Wang, Z.; Li, P.; Li, R. Hypoxia modulation by dual-drug nanoparticles for enhanced synergistic sonodynamic and starvation therapy. J. Nanobiotechnol. 2021, 19, 87.
42. Li, Y.; Hao, L.; Liu, F.; Yin, L.; Yan, S.; Zhao, H.; Ding, X.; Guo, Y.; Cao, Y.; Li, P.; et al. Cell penetrating peptide-modified nanoparticles for tumor targeted imaging and synergistic effect of sonodynamic/HIFU therapy. Int. J. Nanomed. 2019, 14, 5875–5894.
43. Liu, S.; Zhang, W.; Chen, Q.; Hou, J.; Wang, J.; Zhong, Y.; Wang, X.; Jiang, W.; Ran, H.; Guo, D. Multifunctional nanozyme for multimodal imaging-guided enhanced sonodynamic therapy by regulating the tumor microenvironment. Nanoscale 2021, 13, 14049–14066.
44. Du, B.; Yan, X.; Ding, X.; Wang, Q.; Du, Q.; Xu, T.; Shen, G.; Yao, H.; Zhou, J. Oxygen Self-Production Red Blood Cell Carrier System for MRI Mediated Cancer Therapy: Ferryl-Hb, Sonodynamic, and Chemical Therapy. ACS Biomater. Sci. Eng. 2018, 4, 4132–4143.
45. Wang, L.; Song, W.; Choi, S.; Yu, K.; Zhang, F.; Guo, W.; Ma, Y.; Wang, K.; Qu, F.; Lin, H. Hollow CoP@N-Carbon Nanospheres: Heterostructure and Glucose-Enhanced Charge Separation for Sonodynamic/Starvation Therapy. ACS Appl. Mater. Interfaces 2023, 15, 2552–2563.
46. Ma, A.; Chen, H.; Cui, Y.; Luo, Z.; Liang, R.; Wu, Z.; Chen, Z.; Yin, T.; Ni, J.; Zheng, M.; et al. Metalloporphyrin Complex-Based Nanosonosensitizers for Deep-Tissue Tumor Theranostics by Noninvasive Sonodynamic Therapy. Small 2019, 15, e1804028.
47. Guan, S.; Liu, X.; Li, C.; Wang, X.; Cao, D.; Wang, J.; Lin, L.; Lu, J.; Deng, G.; Hu, J. Intracellular Mutual Amplification of Oxidative Stress and Inhibition Multidrug Resistance for Enhanced Sonodynamic/Chemodynamic/Chemo Therapy. Small 2022, 18, e2107160.
48. Neuschmelting, V.; Harmsen, S.; Beziere, N.; Lockau, H.; Hsu, H.T.; Huang, R.; Razansky, D.; Ntziachristos, V.; Kircher, M.F. Dual-Modality Surface-Enhanced Resonance Raman Scattering and Multispectral Optoacoustic Tomography Nanoparticle Approach for Brain Tumor Delineation. Small 2018, 14, e1800740.
49. Salvatori, M.; Rizzo, A.; Rovera, G.; Indovina, L.; Schillaci, O. Radiation dose in nuclear medicine: The hybrid imaging. Radiol. Med. 2019, 124, 768–776.
50. Perry, J.L.; Mason, K.; Sutton, B.P.; Kuehn, D.P. Can Dynamic MRI Be Used to Accurately Identify Velopharyngeal Closure Patterns? Cleft Palate-Craniofacial J. 2018, 55, 499–507.
51. Guo, W.; Chen, Z.; Tan, L.; Gu, D.; Ren, X.; Fu, C.; Wu, Q.; Meng, X. Emerging biocompatible nanoplatforms for the potential application in diagnosis and therapy of deep tumors. View 2021, 3,

20200174.

52. Jennings, L.E.; Long, N.J. ‘Two is better than one’--probes for dual-modality molecular imaging. Chem. Commun. 2009, 24, 3511–3524.
53. Lee, S.Y.; Jeon, S.I.; Jung, S.; Chung, I.J.; Ahn, C.H. Targeted multimodal imaging modalities. Adv. Drug Deliv. Rev. 2014, 76, 60–78.
54. Cai, W.; Chen, X. Multimodality molecular imaging of tumor angiogenesis. J. Nucl. Med. 2008, 49 (Suppl. 2), 113s–128s.